Build Simul (2020) 13: 99–111
https://doi.org/10.1007/s12273-019-0564-y

Urban weather modeling applications: A Vienna case study

Milena Vuckovic (✉), Kristopher Hammerberg, Ardeshir Mahdavi

Department of Building Physics and Building Ecology, TU Vienna, Vienna, Austria

Abstract

Recently, the interest in urban weather modeling methods has been steadily increasing. This is in part due to the insight that thermal building performance simulations are typically undertaken with standardized weather files that provide a rather general perspective on urban weather conditions. This may lead toward errors in conclusions drawn from modeling efforts. In this context, present contribution reports on the potential of different approaches to generate location-dependent urban meteorological data. We compare the meteorological output generated with the Weather Research and Forecasting (WRF) model, Urban Weather Generator, and morphing approach. These methods were compared based on empirical data (air temperature, humidity, and wind speed) collected from two distinct urban locations in Vienna, Austria, over 5 study periods. Our results suggest significant temporal and spatial discrepancies in resulting modeling output. Results further suggest better predictive performance in the case of high-density urban areas and under warmer and extreme conditions in spring and summer periods, respectively.

Keywords

urban climate,
modeling,
dynamic downscaling,
morphing,
data analysis

Article History

Received: 29 August 2018
Revised: 29 May 2019
Accepted: 5 June 2019

1 Introduction

Over the past years, numerous research efforts have been initiated towards the development and refinement of performance assessment tools and methods to support the evaluation of energy demand of the urban building stock (Hong et al. 2000; Foucquier et al. 2013; Fumo 2014; Ghiassi and Mahdavi 2017; Ghiassi et al. 2017). The predictive capabilities of these models depend not only on the capacity of the underlying computational engines, but also on realistic representation of the geometry and zonal complexity of modelled buildings, occupants' presence and behavior, as well as weather conditions. These aspects are often subject to simplifications due to technical challenges regarding data availability and accessibility. For instance, building thermal performance simulations are typically undertaken with standardized (location-independent) weather files usually derived from weather stations in proximity of airports. Such files provide a rather general perspective on the weather conditions in the city (Barnaby and Crawley 2011). However, there is evidence showing that urban developments lead to, among other things, significant heat storage in urban fabric (i.e., building surfaces, pavements, and roads) and micro-level changes in urban climate (see for example, Arnfield 2003; Gaffin et al. 2008; Hagen et al. 2014). Gaffin et al. (2008) noted that intra-urban air temperature variations may be as high as 2 K between the sites that are less than 5 km apart. Thereby, the commonly used standardized weather files are not necessarily representative of the local heat transfer phenomena, location-specific morphologies, anthropogenic emissions, and complex and nonlinear interactions of the surrounding urban fabric and meteorological parameters (Hensen 1999; Pernigotto et al. 2014). As a consequence, the deployment of such files involves various sources of error and may lead to mistakes in building energy systems' specification with negative implications for energy use, indoor thermal comfort, and air quality. For instance, a study conducted by Radhi (2009) has shown that unrealistic representation of external boundary conditions in building performance applications could underestimate annual electricity use by 14.5% and cooling load by 5.9%–8.9%. At the same time, this may increase the operation and maintenance cost of building systems (Hensen 1999; Hong et al. 2013). As such, this calls for development of advance models that can facilitate the assessment and accurate prediction of interactions between the urban structure and local climatic context, towards improved representation of urban weather information in building energy assessments.

E-mail: milena313@gmail.com

1.1 Urban weather modeling

Recently, a wide variety of comprehensive tools for generation of external boundary conditions for building thermal performance models has become available. In general, global circulation models (GCMs), regional weather forecasting models, and computation fluid dynamics (CFD) models have been deployed for the generation of urban microclimatic information (Wilby and Wigley 1997; Rizwan et al. 2008; Mirzaei and Haghighat 2010). However, these methods vary significantly in overall approach, underlying computational methods, informational requirements, and temporal and spatial resolution of the results.

Global and regional models generally rely on the process of downscaling of coarse resolution climate data generated at larger scales, to represent much finer spatial and temporal resolutions. However, downscaling of such data leads to only a probabilistic estimate, rather than a realistic representation of transient phenomena at lower scales (Wilby and Wigley 1997). Together with the time-intensive nature of preparation and execution of such models, and the necessary high level of knowledge, expertise, and experience for properly conducting simulations and interpreting the results, it can be argued that these methods might be less practical for day-to-day utilization in building performance assessment applications. In an attempt to address these shortcomings, one of the recent research efforts concerned the Weather Research and Forecasting (WRF) modeling campaign, within the scope of the ASHRAE Research Project RP-1561, aiming to define a complete mesoscale numerical modeling procedure towards the generation of site-specific meteorological data (Qiu et al. 2015). The WRF model was first run for ten significant climate regions across North America. It was found that the model adequately estimated the observed temperature and humidity data, reasonably well the observed wind, and relatively poorly the observed solar radiation and precipitation data (Qiu et al. 2016). On the grounds of this evaluation, a pre-compiled simplified WRF modeling package (WRF Environmental Modeling System (EMS)) was developed for various terrain categories such as coastal, mountain valleys, mountain plateaus, and major city centers. This package contains a set of user-friendly scripts to support users without advance meteorological knowledge or significant computational resources. This method appears to be a promising alternative to conventional computationally-intensive procedures.

CFD models are another relevant type of prognostic models used to represent local microclimate conditions. CFD models simultaneously solve all the governing equations of fluid dynamics, such as the conservation of mass, momentum, and energy. While CFD models may support relatively fine grid meshes and scale appropriate for urban-scale investigations, the simulation runs are still computationally demanding in terms of both power and time. Therefore, their use in microscale modeling is usually restricted to small domains and relatively simple geometries. A second challenge pertains to the issue of model reliability: Even highly detailed and mathematically consistent simulation tools may yield erroneous results given incomplete (or inaccurate) input data, such as initial/boundary conditions (Maleki et al. 2014). Ideally, an optimization-supported approach should be used toward an empirically based model calibration process (Çetin and Mahdavi 2015, 2016). However, the highly time-intensive simulation runs make comprehensive optimization-based calibration rather infeasible. The high level of domain complexity further aggravates this model reliability problem.

Recently, a focus was given to an alternative approach to generate the local urban weather file. This method involves the process of shifting and stretching of meteorological variables in the present-day weather file, defined here as the baseline climate, to investigate specific phenomena (e.g., projected future climate change, urban heat island (UHI) effect). This technique is referred to as morphing and was used by Belcher at al. (2005) to generate weather data that consider the effects of future climate conditions. Thereby, to preserve the physically realistic temporal sequence of the source data, the present-day weather file is morphed given the predictions from global or regional climate models on monthly mean changes of the meteorological variables. However, the very concept of hour-by-hour adjustments of a source weather data is not a new endeavor and it should probably be attributed to the work of Arens et al. (1980). Later on, the Belcher's approach was adapted by Ren et al. (2014) to incorporate the local UHI effect into the surrounding rural weather data, defined as the baseline climate. For this purpose, a computer-based prognostic meteorological model UCM-TAPM (Urban Canopy Model coupled with a mesoscale climate model TAPM—The Air Pollution Model) was used to provide the required input on changes to monthly mean values of meteorological variables attributable to the effects of the UHI on the urban climate. This method, however, provides only a numerical estimate of the complex and nonlinear interactions of the surrounding urban fabric and meteorological parameters. Hence, the generated files may provide a rather general perspective on the weather conditions in the city.

A further method for generating urban weather information was proposed by Bueno et al. (2012). They developed a meteorological modeling software named Urban Weather Generator (UWG) that derives from meteorological parameters in existing rural weather files corresponding weather representations for locations within the urban fabric. The potential improvement noted in this method, in respect to the ones discussed above, is the consideration of the local urban site morphology (e.g., vegetation coverage,

built area fraction, facade-to-site ratio), buildings' thermal (e.g., albedo, emissivity, conductivity, *U*-value for glazing) and operational properties (e.g., internal heat gain, infiltration, ventilation).

1.2 Overview

Given this background, the present contribution reports on the potential of a number of different approaches for the generation of location-dependent near-surface urban meteorological information for the city of Vienna, Austria. Specifically, we compare the meteorological output generated with Weather Research and Forecasting (WRF) model using the conventional WRF modelling technique, Urban Weather Generator (UWG), and the morphing approach. For this purpose, the following steps were taken:

- Preparation of input parameters and execution of above-mentioned models.
- Investigation of predictive capabilities of the models under various weather conditions. For this purpose, the empirical data pertaining to air temperature, humidity, and wind speed is collected from a number of high-density and low-density urban locations in the city of Vienna, Austria, over 5 distinct time periods.

2 Methodology

2.1 Case study areas

Due to the dynamic evolution of a number of urbanization features, such as overall change of land use, number of buildings, total living floor space, and the number of cars, the city of Vienna, Austria, experienced significant alterations to the local environmental context (Böhm 1998). These changes are usually manifested as potentially considerable micro-level variations in urban climate across the city (Vuckovic et al. 2017). Therefore, these aspects make Vienna an interesting case study to test the prediction accuracy and sensitivity of different climate models to varying urban-scale effects.

To address these circumstances, we focus on two distinct high-density urban (IS) and low-density suburban (DF) typologies within the municipal boundary of the city of Vienna, Austria. These areas vary considerably in terms of their contextual features, as seen in Table 1, implying thus distinctive meteorological conditions. Additionally, a non-urban area (SW), located at the airport at the South-East of Vienna, was selected for the purpose of urban weather modeling efforts.

2.2 Meteorological data

Each study area contains a weather station from a public network, assuring thus a continuous provision of high-resolution meteorological information needed for further analysis. These stations are monitored by the Central Institution for Meteorology and Geodynamics (ZAMG 2018). A more detailed description of the data collection, quality control, and storage procedures of the meteorological observations can be found in Vuckovic et al. (2017, 2018). Table 2 provides an overview of the weather stations and monitoring equipment with information related to the sensor's height above the ground [m]. The deviations from the sensor reference height of 2 m, as suggested by the WMO (2008), are not seen as problematic, as all sensors are positioned within the urban canyon and the vertical gradients are small (Oke 2006). In order to compare wind speed readings taken from different heights, as seen in Table 2, we used the power law to estimate the wind speed at street level at 1.1 m above the ground (Spera and Richards 1979; Bañuelos-Ruedas et al. 2011):

$$\frac{v}{v_n} = \left(\frac{H}{H_n}\right)^{\alpha} \tag{1}$$

where, v is the wind speed at height H = 1.1 m, v_n is the wind speed at height H_n (height of the observations), and α is the friction coefficient (power-law exponent). The friction coefficient used for this study is as follows: 0.25 for non-urban area (SW), 0.30 for mid-density suburban areas (DF), and 0.40 for high-density urban area (IS).

Table 1 General information about the selected locations

Study area	Coordinates	LCZ[1]	Site coverage ratio	Avg. building height [m]	Facade-to-Site ratio[2]	Pervious surface fraction
IS	Lon 16°22′1.00″ Lat 48°11′54.00″	LCZ 2	0.43	20.64	1.50	0.11
DF	Lon 16°26′11.04" Lat 48°15′26.56"	LCZ 6	0.23	6.67	0.42	0.52
SW	Lon 16°34′15.0″ Lat 48°06′39.0″	LCZ D_E	0	0	0	0.81

[1] LCZ stands for Local Climate Zone, a classification system devised by Stewart and Oke (2012).

[2] Details regarding the urban morphology parameters can be found in Bueno et al. (2013).

Table 2 Overview of the monitoring equipment with information about the height of the sensors (meters above the ground)

Weather station	Station elevation [m]	Temperature [°C]	Relative humidity [%]	Wind speed [m·s^{-1}]
IS	177	9.3	9.3	52
DF	161	2	2	13
SW	184	2.2	2.2	10

2.3 Study periods

In order to investigate the predictive capabilities of concerned modeling approaches over different weather conditions, we used *k*-means cluster analysis to select 5 distinct time periods from acquired hourly-based meteorological dataset (air temperature, humidity, wind speed, solar radiation, and precipitation) representing the year 2015. These representative periods were clustered based on measurements taken at the SW weather station, which is located at an open site that allows atmospheric mixing, making it well suited for generalizing the regional weather condition with a clustering approach. Clustering was performed using three uncorrelated key meteorological indicators: temperature, diurnal temperature range, and wind speed, whereby the number of considered clusters varied from 2 to 10. It was noted that when more than 5 clusters were selected, noticeable distinctions between the categories disappeared. Therefore, 5 weather clusters were selected to provide the widest range of distinct weather typologies. The most representative period within each cluster was taken as the 48-hour timeframe that had values furthest from the mean values of the other 4 clusters (Table 3). This approach ensured that each modeled period represents the aspects that make that cluster distinct from the others. Taking the period with values closest to the cluster's mean resulted in dates that were not sufficiently differentiated from one another. By selecting the more distinct cases, the performance of the models could be examined under a wider range of weather conditions.

Table 3 Representative dates and key meteorological indicators

Period	Mean temperature [°C]	Diurnal range [K]	Mean wind speed [m·s^{-1}]
January 7– 8	−1.6	5.1	1.6
February 8–9	−0.3	4.3	5
March 20–21	6.9	15.2	0.7
April 21–22	15	12.3	2.5
July 5–6	27.3	16.1	1.6

2.4 WRF model

The Weather Research and Forecasting (WRF) model is a mesoscale numerical weather prediction (NWP) and atmospheric simulation system (Skamarock et al. 2008; WRF 2018). WRF has been designed to provide a spectrum of capabilities ranging from global scale to large eddy simulations (Chen et al. 2011; Ercolani et al. 2015). For the purpose of this study we used WRF version 3.2. The WRF model requires a large number of input data to initialize the model. First, a land cover map was generated using the World Urban Database and Access Portal Tool (WUDAPT) methodology (Hammerberg et al. 2017, 2018) and the Local Climate Zone (LCZ) concept developed by Stewart and Oke (2012). Random Forest Classification algorithm (Bechtel et al. 2015) was deployed to classify the Landsat satellite imagery to best represent each LCZ class. The algorithm uses the distinct reflective signature in each spectral band to classify each 100 m × 100 m pixel within the region of interest. For each LCZ class in the land cover map a morphological description or urban canopy parameters (e.g., height-to-width ratio, pervious surface fraction, average building height) was provided, as required by the sub-grid urban model within the WRF, named the Building Effect Parameterization and Building Energy Model—BEP+BEM (Martilli et al. 2002; Salamanca et al. 2010). The respective urban canopy parameters representing each LCZ class are discussed in detail in Stewart and Oke (2012). More detailed description depicting the step-by-step land cover mapping procedure is provided in Hammerberg et al. (2018). The operational building parameters, such as the occupancy schedules and thermal properties of the building envelope, were left as default values. To facilitate a dynamic representation of the land-atmosphere interactions, a number of parameterization schemes were used. The Bougeaut-Lacarrère 1.5-order turbulence scheme was used for the planetary boundary layer representation (Bougeault and Lacarrere 1989). Lateral boundary weather conditions, as initial and boundary conditions, were taken from the NCEP's FNL (Final) Operational Global Analysis dataset (NCEP 2018) at an interval of six hours on a 1° by 1° grid for each 2-day simulation with a spin-up time of six hours. The USGS global elevation datasets were used for the topography input (GTOPO30 2018). Additional model configuration parameters can be found in Table 4. It should be noted that the focus of our study was to evaluate how the model would perform in a predictive capacity using only larger boundary conditions as the input. Therefore, our methodology does not consider the nudging via observational weather data, reducing thus both complexity of the model runs and overall simulation time.

Once the model was configured and the initial conditions set, the WRF model was run and results for selected study areas isolated. Three nested domains were used to downscale the results to an inner domain with a 500 m resolution, whereby for each 500 m × 500 m grid only a single LCZ

Table 4 WRF model configuration

Shortwave radiation	Dudhia scheme
Longwave radiation	RRTM scheme
Microphysics	WRF Single-Moment 6-class scheme
Cumulus parameterization	—
Planetary boundary layer	Bougeaut-Lacarrère
Surface layer	MM5 similarity
Land surface	Noah Land Surface Model
Urban physics	BEP+BEM
Boundary conditions	NCEP FNL Global Analysis (ds 083.2)
Time step	30 s
Number of vertical layers	51

classification with specific land use and built typology is assigned.

2.5 UWG model

As mentioned at the outset, UWG is a meteorological modeling software that, given a specific set of urban canopy parameters, modifies the hourly values of air temperature and relative humidity in existing rural weather files (Bueno et al. 2013). To facilitate the process, we used the morphological parameters previously generated for the purpose of the WRF model, for the same spatial domain (500 m × 500 m) and the two study areas (as seen in Table 1). The operational and thermal building parameters were derived based on the usage and vintage. Building use was categorized broadly as residential and commercial. Austrian OIB standards were followed when determining the construction periods (OIB 2015). Using the geospatial data provided by the city of Vienna, the distributions of these representative building categories were identified within each domain. Altogether, four construction periods were considered with six building typologies, as seen in Tables 5 and 6. Thermal material properties were assigned based on construction age as defined in the OIB standards (OIB 2015). Operational building properties, such as the hourly-based occupancy profiles based on building use, were adopted from the ASHRAE standards (ASHRAE 2013). The related building energy use and internal gains were then calculated according to the ÖNORM standards (ÖNORM 2011), as seen in Table 7.

It should be noted, however, that UWG tool currently allows only four building categories to be defined at the time, each representing exactly 25% of the whole building stock within an area of inquiry. In other words, the distribution of building typologies could only be defined in increments of 25%. The resulting representation of the surrounding urban features is thus subject to simplification, which might affect the modeling results.

2.6 Morphing approach

For the purpose of urban weather modeling using the

Table 5 Building typology and thermal material properties according to the usage and vintage

Construction period	Typology	Glazing ratio	Window U-value [W·m^{-2}·K^{-1}]	Albedo (wall)	Albedo (roof)	Emissivity (wall)	Emissivity (roof)
Before 1900	Residential 1	0.15	2.50	0.45	0.28	0.91	0.90
1900–1945	Residential 2						
1945–1976	Residential 3	0.15	3.00	0.45	0.16	0.91	0.28
Before 1900	Commercial 1	0.15	2.50	0.45	0.28	0.91	0.90
1900–1945	Commercial 2						
After 1976	Commercial 3	0.30	3.00	0.45	0.18	0.91	0.92

Table 6 Distribution of representative building typologies (represented in increments of 25%) for two study urban areas IS and DF

Location	I	II	III	IV
IS	Residential 1	Residential 2	Commercial 1	Commercial 2
DF	Residential 3	Residential 3	Commercial 3	Commercial 3

Table 7 Operational building properties based on building typology

Typology	Daytime internal gains [W·m^{-2}]	Nighttime internal gains [W·m^{-2}]	Ventilation rate [h^{-1}]	Daytime cooling set point [°C]	Nighttime cooling set point [°C]	Daytime heating set point [°C]	Nighttime heating set point [°C]
Residential	5.4	12.0	0.4	26	28	20	17
Commercial	33.2	1.8	1.2				

morphing approach, the hourly-based rural weather file obtained from the location SW was used as the baseline climate. The average monthly changes of meteorological variables attributable to the effects of urbanization were computed based on the empirical meteorological data obtained from two study urban areas IS and DF. Tables 8 and 9 provide the information regarding the weather statistics from two urban study areas.

In the original approach developed by Belcher et al. (2005) the information regarding the urban weather statistics (monthly mean, maximal, minimal values of meteorological parameters) is estimated using the global climate models. However, due to the time-intensive nature of the WRF simulations, for the purpose of this study the model was run only for five key date ranges previously defined using the weather cluster analysis.

The process of shifting and stretching of meteorological variables was incorporated by applying the morphing method developed by Belcher et al. (2005) and further adapted by Ren et al. (2014):

$$T = T_o + \Delta T_m + \alpha_{Tm}\left(T_o - \left\langle T_o \right\rangle_m\right) \quad (2)$$

$$\alpha_{Tm} = \frac{\Delta T_{MAXm} - \Delta T_{MINm}}{\left\langle T_{omax} \right\rangle_m - \left\langle T_{omin} \right\rangle_m} \quad (3)$$

$$RH = RH_0\left(1 + \alpha_{Rm}\right) \quad (4)$$

$$v = v_0\left(1 + \alpha_{Vm}\right) \quad (5)$$

where, T and T_o are the hourly urban and rural ambient air temperatures, respectively. $\left\langle T_o \right\rangle_m$, $\left\langle T_{omax} \right\rangle_m$, $\left\langle T_{omin} \right\rangle_m$ are the monthly mean values of the ambient air temperature, daily maximum temperature and daily minimum temperature, respectively, from the rural weather data. ΔT_m, ΔT_{MAXm}, ΔT_{MINm} are the differences between the urban and the rural areas in monthly mean ambient air temperature, maximum temperature and minimum temperature, respectively. As mentioned above, these are computed from urban weather data obtained at locations IS and DF. RH and RH_0 are the hourly urban and rural relative humidity values, respectively. v and v_0 are the hourly urban and rural wind speed, respectively. α_{Tm}, α_{Rm}, α_{Vm} are the fractional monthly changes of temperature, relative humidity, and wind speed, respectively, between urban and rural areas. Once the combination of a shift and a stretch from the rural weather file is applied, the urban weather file is computed.

2.7 Comparison between the models

Tables 10 and 11 summarize the key differences in modeling techniques, inputs, and outputs for all three models used in this study. It can be observed that not all meteorological

Table 8 Information regarding the air temperature for all study areas

	Min temperature [°C]			Average temperature [°C]			Max temperature [°C]		
Location	IS	DF	SW	IS	DF	SW	IS	DF	SW
January	−3.6	−4.0	−6.1	4.1	3.6	2.7	17.7	17.7	17.3
February	−2.2	−4.1	−5.3	3.3	2.4	2.0	10.9	10.7	11.3
March	1.3	−1.9	−3.7	7.8	6.9	6.3	16.7	16.2	17.3
April	1.7	0.6	−2.1	12.5	11.5	10.9	26.4	26.0	25.5
May	9.0	6.1	5.9	16.3	15.6	15.1	26.6	26.3	25.7
June	12.0	10.7	8.3	20.9	20.2	19.5	32.4	31.8	31.3
July	14.0	11.3	10.5	25.1	24.3	23.7	37.5	36.7	35.9
August	14.7	11.9	10.0	24.9	24.1	23.3	36.8	37.0	35.6

Table 9 Information regarding the relative humidity and wind speed (at 10 m above the ground) for all study areas

	Min RH [%]			Max RH [%]			Min wind [m·s^{-1}]			Max wind [m·s^{-1}]		
Location	IS	DF	SW	IS	DF	SW	IS	DF	SW	IS	DF	SW
January	40	45	42	95	93	100	0.1	0.0	0.1	6.3	8.9	16.0
February	36	41	33	94	93	100	0.1	0.1	0.1	4.6	7.1	13.3
March	27	30	30	89	92	97	0.0	0.0	0.1	4.3	7.6	12.9
April	19	25	19	91	94	96	0.1	0.0	0.3	4.0	7.2	13.3
May	27	34	31	95	92	99	0.1	0.0	0.1	3.2	5.1	10.4
June	26	32	26	89	92	97	0.0	0.0	0.3	3.9	4.7	10.3
July	18	28	20	88	91	95	0.0	0.0	0.1	4.5	4.5	11.4
August	15	26	19	94	91	100	0.0	0.0	0.2	3.8	4.7	11.4

Table 10 Comparison between the modeling techniques and input data requirements

	WRF	UWG	Morphing
Modeling techniques	Dynamic downscaling	Bottom-up building stock model based on energy conservation principles	Hour-by-hour adjustments of the source weather data
Input data requirements	Three-dimensional limited area model is driven with the GCM output (initial and boundary conditions), physics options describing various physics modules, urban canopy representation, domain size	The model takes input parameters that describe urban morphology and vegetation coverage, building surface materials, building operational properties, boundary layer parameters, and domain size	The predictions from global or regional climate models on monthly mean changes of the meteorological variables are fed into a set of equations that account for shifting and stretching of meteorological variables

Table 11 Comparison between the selected model outputs

Parameter	WRF	UWG	Morphing
Air temperature	✓	✓	✓
Relative humidity	✓	✓	✓
Wind speed	✓	—	✓
Wind direction	✓	—	—
Solar radiation	✓	—	✓
Precipitation	✓	—	✓

parameters are considered by all the models (Table 11). As it was mentioned before, UWG model is capable of estimating the urban air temperature and relative humidity values, while other parameters are inherited from the reference rural weather file. On the other hand, WRF and morphing approach are capable of modeling a number of meteorological parameters, however using different modeling techniques (as seen in Table 10).

It should be noted, however, that as the meteorological data obtained from selected non-urban location (SW) do not include solar radiation data, it is not possible to derive the information regarding the adjusted solar radiation for two study urban areas using the morphing approach. Having in mind the current limitations of the UWG model's output, this allows us, in principle, to evaluate the solar output only from WRF model against the observed data. Given this circumstance, our further analysis focused on comparison of air temperature, absolute humidity, and wind data generated with these alternative approaches.

3 Results and discussion

3.1 Air temperature

The results show high seasonal fluctuations and significant deviations of the modeling output compared to the empirical observations for both study areas (Fig. 1). Due to the nature of the cluster analysis and date selection process each study period represents a unique combination of climate conditions. Thereby, it may be observed that the WRF model displays better predictive performance under warmer and extreme conditions in spring and summer periods, respectively. The periods in January and March were the worst performing periods for the WRF model with the highest RMSE and mean absolute error for both areas (Tables 12 and 13). These periods were the most atmospherically stable with the least mixing due to the lower recorded average wind speed (Table 3). However, the period of March also had the second largest diurnal temperature range. This combination of conditions increases the impact of local urban microclimate effects and thus exacerbates errors of localization in both the representation of the urban surroundings and the representativeness of weather stations. This leads to increasing the prediction error in the model. The period of February, on the other hand, had the highest recorded wind speed (5 $m \cdot s^{-1}$) and the lowest diurnal temperature variation. This indicates more thoroughly mixed conditions that would be less influenced by local effects. The results also indicate the tendency of the WRF model to overestimate the air

Table 12 Performance of the models for air temperature predictions (W, U, M stand for WRF, UWG, morphing approach, respectively) for location IS

Metric	RMSE			Mean absolute error [K]			Mean bias		
Model	W	U	M	W	U	M	W	U	M
January 7– 8	3.9	0.9	0.6	3.2	0.8	0.5	−3.2	0.7	−0.3
February 8–9	1.7	0.5	1.6	1.4	0.4	1.5	0.9	0.0	1.5
March 20–21	4.7	1	1.7	3.9	0.8	1.5	3.9	0.0	−0.9
April 21–22	1.4	1.3	0.9	1.1	1.1	0.6	−0.1	−1.0	−0.3
July 5–6	2.1	1.7	2.2	1.6	1.4	1.8	0.4	−0.8	−0.7

Table 13 Performance of the models for air temperature predictions (W, U, M stand for WRF, UWG, morphing approach, respectively) for location DF

Metric	RMSE			Mean absolute error [K]			Mean bias		
Model	W	U	M	W	U	M	W	U	M
January 7–8	3.3	0.9	0.5	2.6	0.9	0.5	−2.6	0.6	0.0
February 8–9	1.7	0.5	0.7	1.3	0.3	0.6	0.9	−0.2	0.5
March 20–21	4.6	2.6	1.2	4.0	2.2	1.0	4.0	1.2	−0.1
April 21–22	1.4	1.4	0.8	1.1	1	0.7	−0.3	−0.4	−0.1
July 5–6	1.8	1.9	1.7	1.6	1.6	1.2	0.1	−0.2	−0.2

temperature. This might be due to the limitations of the WRF model related to the LCZ classification with specific land use and built typology for each grid, simplifying the occupancy representation and anthropogenic heat output, affecting thus the temperature rise.

The results further indicate that the air temperature output from the UWG and morphing models is closer to the monitored data, when compared to the output from the WRF model. This is further supported by the lower RMSE for both models (Tables 12 and 13). Additionally, both models show a potential for more accurate representation of the daily temperature ranges and fluctuations compared to the WRF model. However, UWG model tends to underestimate air temperature (Fig. 1), which is particularly evident under atmospherically stable periods. A comparison of the two study areas reveals a better performance of the UWG model for high-density urban area (IS). This might be due to the fact that the model was found to perform better in areas in which the urban morphology is relatively homogeneous and the urban vegetation is scarce (Bueno et al. 2013), as is the case for IS. The output from the morphing approach reveals poor performance under unstable weather conditions with higher atmospheric mixing, due to the higher recorded average wind speed of around 5 $m \cdot s^{-1}$, with the tendency to overestimate the air temperature. Furthermore, under extreme weather conditions and higher air temperatures, the model tends to underestimate the air temperature. A slightly better performance of the model was observed for the low-density urban area (DF).

3.2 Humidity

All three models tend to underestimate the absolute humidity in nearly every study period in the case of the low-density

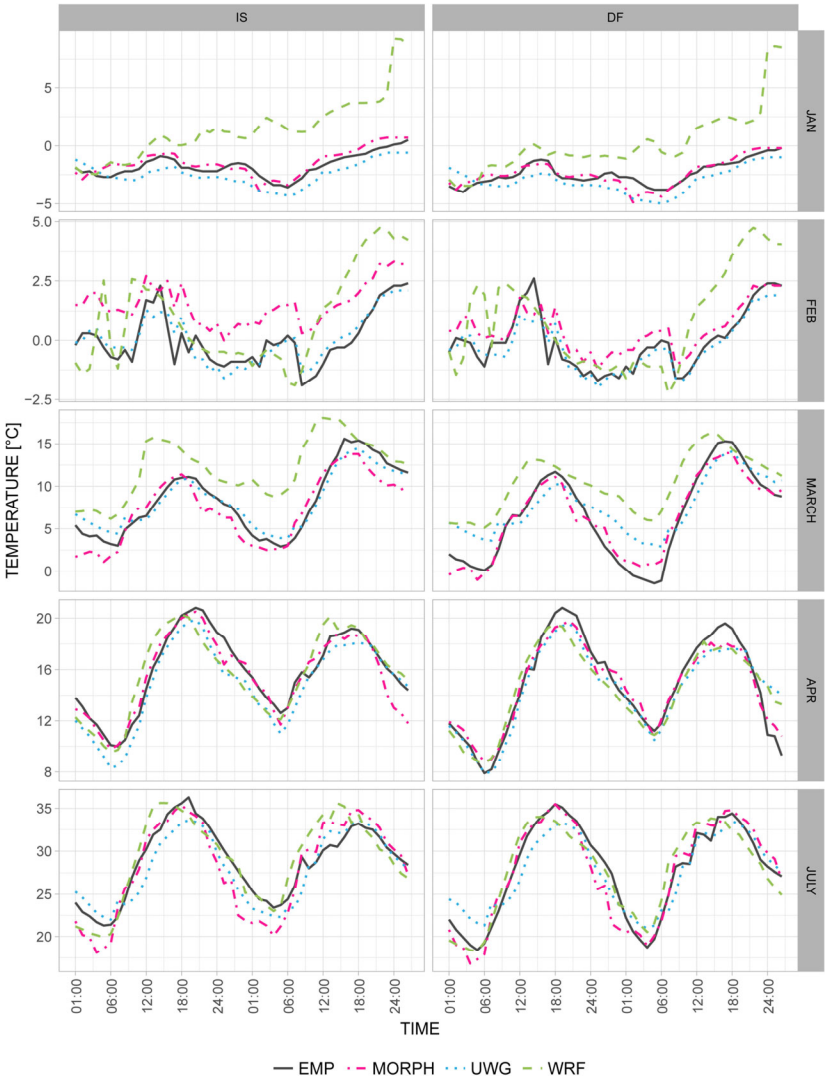

Fig. 1 Hourly distribution of air temperature from WRF, UWG and morphing approach compared to empirically obtained data (EMP) for urban areas IS (left) and DF (right)

urban area DF (Fig. 2). The reverse trend may be observed for the high-density urban area IS, except for the period of February. In general, a better fit to the empirical data is observed for the location IS. This may be due to the lower pervious surface fraction (Table 1) and overall low amount of water vapor present in the air and therefore less variability across the area.

July had the highest value and the most variation in specific humidity. It was also the period that all models showed the least agreement with measured values, which is further supported by high RMSE (Tables 14 and 15). This is especially evident for the low-density urban area DF. This indicates that all models have difficulties predicting humidity levels during periods of high variability. In general, the differences in absolute humidity between the models and observations were less extreme and less varied than near-surface air temperature.

3.3 Wind speed

The results indicate that the wind speed output from WRF model and morphing approach are closer to the monitored data in the case of high-density urban area IS (Fig. 3). This is further supported by lower RMSE and mean absolute error for both models for this area, as seen in Tables 16 and 17. This might be due to the overall decrease of airflow in location IS, due to the dense arrangement of built structures, and a somewhat smaller tendency toward extreme fluctuations of wind speed during the day. It should be noted that the UWG model currently modifies only the air temperature and humidity in existing rural weather files (Bueno et al. 2013).

The period in February was the worst performing period for both models with the highest RMSE and mean absolute error for both areas. As it was already mentioned,

Fig. 2 Hourly distribution of absolute humidity from WRF, UWG and morphing approach compared to empirically obtained data (EMP) for urban areas IS (left) and DF (right)

Table 14 Performance of the models for absolute humidity predictions (W, U, M stand for WRF, UWG, morphing approach, respectively) for location IS

Metric	RMSE			Mean absolute error [g·m^{-3}]			Mean bias		
Model	W	U	M	W	U	M	W	U	M
January 7- 8	0.7	0.3	0.2	0.5	0.2	0.2	−0.5	0.2	−0.1
February 8-9	0.5	0.2	0.2	0.4	0.1	0.2	−0.1	0.0	−0.2
March 20-21	0.3	0.4	0.3	0.3	0.3	0.2	0.1	0.0	−0.1
April 21-22	0.5	0.7	0.5	0.4	0.6	0.4	0.1	0.5	0.3
July 5-6	0.9	1.0	1.0	0.8	0.8	0.8	0.0	0.5	0.1

Table 15 Performance of the models for absolute humidity predictions (W, U, M stand for WRF, UWG, morphing approach, respectively) for location DF

Metric	RMSE			Mean absolute error [g·m^{-3}]			Mean bias		
Model	W	U	M	W	U	M	W	U	M
January 7–8	0.7	0.2	0.6	0.5	0.2	0.6	−0.5	0.1	0.6
February 8–9	0.5	0.3	0.8	0.4	0.2	0.7	0.1	0.0	−0.7
March 20–21	0.4	0.4	0.5	0.3	0.3	0.5	0.1	0.0	−0.5
April 21–22	0.7	0.5	1.1	0.6	0.4	1.0	−0.5	−0.1	−1.0
July 5–6	2.2	1.7	3.8	2.0	1.5	3.7	−2.0	−1.5	−3.7

February was the period characterized by strong turbulent motions with average wind speed of around 5 m·s^{-1} (Table 3). This suggests that both models may experience difficulties when predicting wind speed during periods of high turbulence. However, the deviations in wind speed predictions from the empirical observations were small when compared to the near-surface air temperature and absolute humidity predictions.

4 Discussion and conclusion

The present contribution reported on the potential of three alternative approaches (WRF, UWG, and morphing approach) towards generation of near-surface urban meteorological information (2 m height above the ground) pertaining to the air temperature, absolute humidity, and wind speed, for two urban areas in the city of Vienna, Austria. The results were compared based on empirical data obtained from these two areas. In this study, the results were further compared based on the indicators such as RMSE, Mean Absolute Error, and Mean Bias. The results revealed significant spatial and temporal differences between the generated meteorological output with air temperature showing the highest deviation from the empirically collected data. The results further indicated that the meteorological output from the UWG and morphing models is closer to the monitored data, when compared to the output from the WRF model. This was more prominent in the case of near-surface temperature predictions. The results also indicated the tendency of the WRF model to overestimate the air temperature, especially during the colder and atmospherically stable periods. The temperature output from the morphing approach revealed poor performance under unstable weather conditions with high atmospheric mixing. In general, results suggested better predictive performance of the models in the case of high-density urban area and under warmer and extreme conditions in spring and summer periods, respectively.

Additionally, all models faced difficulties predicting humidity levels during periods of high variability observed in July. This was especially evident for the low-density urban area. It was also noted that all three models tend to underestimate the absolute humidity in nearly every study period in the case of the low- density urban area, with morphing approach being the worst performing. However, the WRF model had the highest RMSE and mean absolute error for the majority of humidity predictions.

The best fit to the observed values was noted in the case of wind speed predictions. However, during periods with a higher degree of atmospheric mixing and strong turbulent motions, as observed in February, WRF model and morphing approach experienced significant difficulties with a tendency to overestimate the wind speed values.

Since the output from the WRF model displayed significant discrepancies from the empirical data obtained for specific domains considered in this contribution, we cannot identify the WRF model as an appropriate tool for deriving urban boundary conditions for building energy modeling. Furthermore, the deployment of this tool is rather time-intensive by nature and requires a high degree of manual user intervention and expertise. This makes it less practical for day-to-day utilization in building design support applications. However, one needs to keep in mind that as the nudging option was not used, this might be one of the reasons behind the observed errors in WRF output, allowing thus the model to drift from reality. Additionally, as the ground weather stations that provided observational data are likely not positioned exactly at the center point of the grid cells (in case of both urban areas) in the WRF model, the near morphological surroundings may slightly differ, causing thus deviations between observed and modeled meteorological parameters. It should be also noted that studies often run the WRF simulations using different land-use data or different time periods (under current and future scenarios) to analyze the performance of the WRF model in respect to varying input parameters (Jiang et al. 2008; Sharma et al. 2014). This approach allows, in principle, for the most optimal setup of the model to be identified, while also driving the variations in modeling output. Likewise, a study done by Mauree et al. (2018) demonstrated that with the improvement of the surface representation in the WRF model, using for example the advanced canopy interface

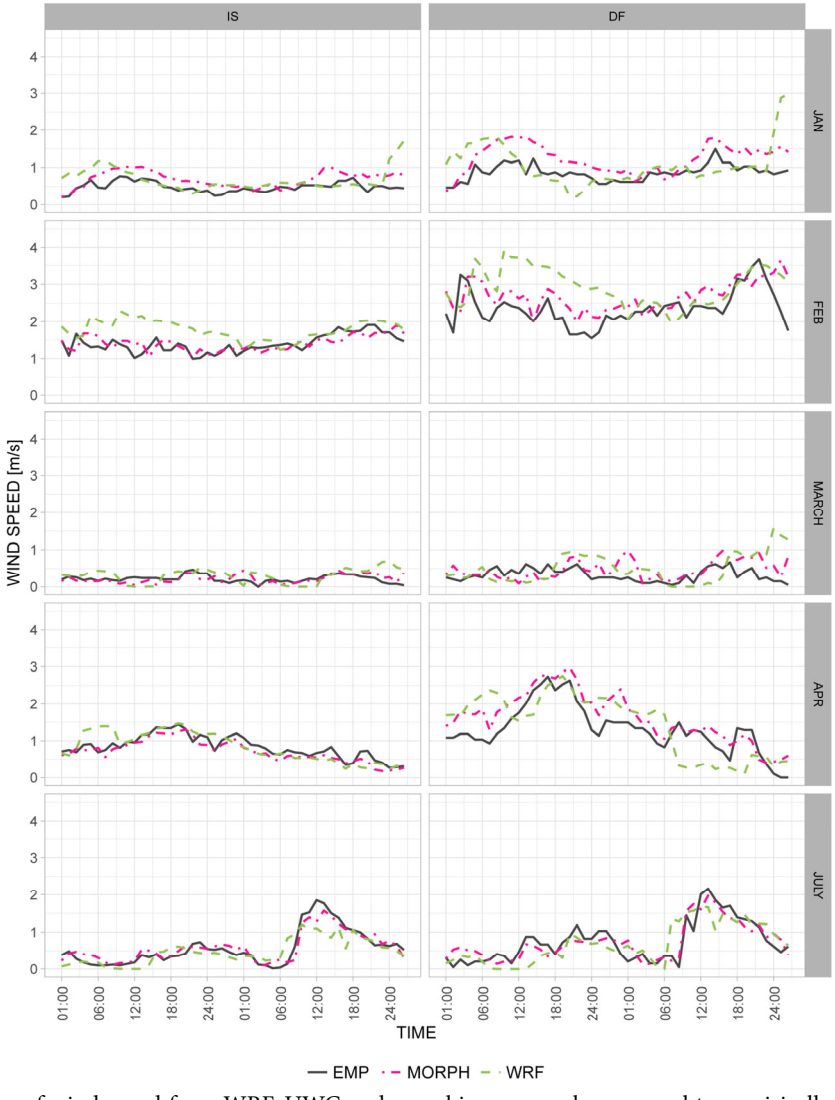

Fig. 3 Hourly distribution of wind speed from WRF, UWG and morphing approach compared to empirically obtained data (EMP) for urban areas IS (left) and DF (right)

Table 16 Performance of the models for wind speed predictions (W, M stand for WRF, morphing approach, respectively) for location IS

Metric	RMSE		Mean absolute error [m·s^{-1}]		Mean bias	
Model	W	M	W	M	W	M
January 7–8	0.4	0.3	0.2	0.2	−0.2	−0.2
February 8–9	0.5	0.2	0.4	0.2	0.4	0.0
March 20–21	0.1	0.2	0.2	0.1	0.1	0.0
April 21–22	0.2	0.2	0.2	0.1	0.0	−0.1
July 5–6	0.3	0.2	0.2	0.1	−0.1	0.0

Table 17 Performance of the models for wind speed predictions (W, M stand for WRF, morphing approach, respectively) for location DF

Metric	RMSE		Mean absolute error [m·s^{-1}]		Mean bias	
Model	W	M	W	M	W	M
January 7– 8	0.6	0.4	0.4	0.4	−0.2	−0.4
February 8–9	0.9	0.5	0.7	0.4	0.6	0.3
March 20–21	0.5	0.3	0.4	0.2	0.2	0.1
April 21–22	0.7	0.4	0.6	0.4	0.1	0.3
July 5–6	0.4	0.3	0.3	0.2	−0.1	0.0

model (CIM), deviations from the observed meteorological data are significantly reduced. This is namely due to the consideration of horizontal fluxes in the CIM calculations. This method may also improve the computational time. However, in our study, the more easily deployable alternatives, such as the UWG and morphing approach, appear to give more satisfactory results. However, due to the current limitations of the UWG tool to modify only two specific meteorological parameters (air temperature and humidity), the deployment of such simplified weather files may have

major implications for simulation-supported assessment of buildings' thermal performance and, consequently, their environmental impact. Lastly, since the morphing approach relies on the output from a global or a regional model, which in this case was proven to perform poorly, the suitability of these files may also be debatable.

Note that the above conclusions and observations are obviously limited, given the fact that the described model comparison effort was restricted only to one city. Nonetheless, it appears that, while the work done by the urban climate research community over the past decade has been rather extensive, there is ample room for further improvements and additional developments regarding tools and methods for high-resolution urban climate modeling.

Funding note: Open access funding provided by TU Vienna.

References

Arens EA, Flynn LE, Nall DN, Ruberg K (1980). Geographical extrapolation of typical hourly weather data for energy calculation in buildings. National Bureau of Standards.

Arnfield AJ (2003). Two decades of urban climate research: A review of turbulence, exchanges of energy and water, and the urban heat island. *International Journal of Climatology*, 23: 1–26.

ASHRAE (2013). ASHRAE Standard 90.1, User's Manual. Atlanta: American Society of Heating, Refrigerating and Air-Conditioning Engineers.

Bañuelos-Ruedas F, Angeles-Camacho C, Rios-Marcuello S (2011). Methodologies used in the extrapolation of wind speed data at different heights and its impact in the wind energy resource assessment in a region. In: Suvire GO (ed), Wind Farm—Technical Regulations, Potential Estimation and Siting Assessment, Chaper 4. London: InTech.

Barnaby CS, Crawley DB (2011). Weather data for building performance simulation. In: Hensen JLM, Lamberts R (eds), Building Performance Simulation for Design and Operation, Chapter 3. New York: Taylor & Francis.

Bechtel B, Alexander P, Böhner J, Ching J, Conrad O, Feddema J, Mills G, Linda SE, Stewart I (2015). Mapping local climate zones for a worldwide database of the form and function of cities. *ISPRS International Journal of Geo-Information*, 4: 199–219.

Belcher S, Hacker JN, Powell DS (2005). Constructing design weather data for future climates. *Building Services Engineering Research and Technology*, 26: 49–61.

Böhm R (1998). Urban bias in temperature time series—A case study for the city of Vienna, Austria. *Climatic Change*, 38: 113–128.

Bougeault P, Lacarrere P (1989). Parameterization of orography-induced turbulence in a mesobeta-scale model. *Monthly Weather Review*, 117: 1872–1890.

Bueno B, Norford L, Hidalgo J, Pigeon G (2013). The urban weather generator. *Journal of Building Performance Simulation*, 6: 269–281.

Chen F, Kusaka H, Bornstein R, Ching J, Grimmond CSB, Grossman-Clarke S, Loridan T, Manning KW, Martilli A, Miao SG, Sailor D, Salamanca FP, Taha H, Tewari M, Wang X, Wyszogrodzki AA, Zhang C (2011). The integrated WRF/urban modelling system: Development, evaluation, and applications to urban environmental problems. *International Journal of Climatology*, 31: 273–288.

Çetin R, Mahdavi A (2015). An empirically-based assessment of CFD utility in urban-level air flow studies. In: Proceedings of the 14th International IBPSA Building Simulation Conference, Hyderabad, India.

Çetin R, Mahdavi A (2016). An inquiry into the reliability of urban-level CFD-based air flow field analysis. In: Proceedings of Central European Symposium on Building Physics CESBP 2016/BauSIM, Dresden, Germany.

Ercolani G, Gorlé C, García-Sánchez C, Corbari C, Mancini M (2015). RAMS and WRF sensitivity to grid spacing in large-eddy simulations of the dry convective boundary layer. *Computers & Fluids*, 123: 54–71.

Foucquier A, Robert S, Suard F, Stéphan L, Jay A (2013). State of the art in building modelling and energy performances prediction: A review. *Renewable and Sustainable Energy Reviews*, 23: 272–288.

Fumo N (2014). A review on the basics of building energy estimation. *Renewable and Sustainable Energy Reviews*, 31: 53–60.

Gaffin SR, Rosenzweig C, Khanbilvardi R, Parshall L, Mahani S, Glickman H, Goldberg R, Blake R, Slosberg RB, Hillel D (2008). Variations in New York city's urban heat island strength over time and space. *Theoretical and Applied Climatology*, 94: 1–11.

Ghiassi N, Mahdavi A (2017). Reductive bottom-up urban energy computing supported by multivariate cluster analysis. *Energy and Buildings*, 144: 372–386.

Ghiassi N, Tahmasebi F, Mahdavi A (2017). Harnessing buildings' operational diversity in a computational framework for high-resolution urban energy modeling. *Building Simulation*, 10: 1005–1021.

GTOPO30 (2018). Global 30 Arc-Second Elevation, The Long Term Archive. Available at https://lta.cr.usgs.gov/GTOPO30. Accessed: 07 Feb 2018.

Hagen K, Gasienica-Wawrytko B, Loibl W, Pauleit S, Stiles R, Tötzer T, Trimmel H, Köstl M, Feilmayr W (2014). Smart environment for smart cities: Assessing urban fabric types and microclimate responses for improved urban living conditions. In: Proceedings of the REAL CORP 2014, Vienna, Austria.

Hammerberg K, Brousse O, Mahdavi A (2017). Investigating the suitability of the WRF model for improving prediction of urban climate boundary conditions. In: Proceedings of the Building Simulation Applications, Bozen Bolzano, Italy.

Hammerberg K, Brousse O, Martilli A, Mahdavi A (2018). Implications of employing detailed urban canopy parameters for mesoscale climate modelling: a comparison between WUDAPT and GIS databases over Vienna, Austria. *International Journal of Climatology*, 38: e1241–e1257.

Hensen JLM (1999). Simulation of building energy and indoor environmental quality—Some weather data issues. In: Proceedings of the International workshop on climate data and their applications in engineering, Prague, Czech Republic.

Hong T, Chou S, Bong T (2000). Building simulation: An overview of developments and information sources. *Building and Environment*, 35: 347–361.

Hong T, Chang W, Lin H (2013). A fresh look at weather impact on peak electricity demand and energy use of buildings using 30-year actual weather data. *Applied Energy*, 111: 333–350.

Jiang X, Wiedinmyer C, Chen F, Yang Z-L, Lo JC-F (2008). Predicted impacts of climate and land use change on surface ozone in the Houston, Texas, area. *Journal of Geophysical Research*, 113: D20312.

Maleki A, Kiesel K, Vuckovic M, Mahdavi A (2014). Empirical and computational issues of microclimate simulation, In: Proceedings of ICT EurAsia 2014, Indonesia.

Martilli A, Clappier A, Rotach MW (2002). An urban surface exchange parameterisation for mesoscale models. *Boundary-Layer Meteorology*, 104: 261–304.

Mauree D, Blond N, Clappier A (2018). Multi-scale modeling of the urban meteorology: Integration of a new canopy model in the WRF model. *Urban Climate*, 26: 60–75.

Mirzaei PA, Haghighat F (2010). Approaches to study urban heat island – abilities and limitations. *Building and Environment*, 45: 2192–2201.

NCEP (2018). Available at https://rda.ucar.edu/datasets/ds083.2/#!description. Accessed 07 Feb 2018.

OIB (2015). OIB-RL 6, Energietechnisches Verhalten von Gebäuden, OIB-330.6-011/15.

Oke TR (2006). Towards better scientific communication in urban climate. *Theoretical and Applied Climatology*, 84: 179–190.

ÖNORM (2011). ÖNORM B 8110-5, Wärmeschutz im Hochbau.

Pernigotto G, Prada A, Cóstola D, Gasparella A, Hensen JLM (2014). Multi-year and reference year weather data for building energy labelling in North Italy climates. *Energy and Buildings*, 72: 62–72.

Qiu X, Yang F, Corbett-Hains H, Roth M (2015). Procedure to adjust observed climatic data for regional or mesoscale climatic variations. Final Report of ASHRAE Research Project 1561-RP. Atlanta: American Society of Heating, Refrigerating and Air-Conditioning Engineers.

Qiu X, Roth M, Corbett-Hains H, Yang F (2016). Mesoscale climate modeling procedure development and performance evaluation. ST-16-019 (RP-1561), ASHRAE Annual Conference, St. Louis, MO, USA.

Radhi H (2009). A comparison of the accuracy of building energy analysis in Bahrain using data from different weather periods. *Renewable Energy*, 34: 869–875.

Ren Z, Wang X, Chen D, Wang C, Thatcher M (2014). Constructing weather data for building simulation considering urban heat island. *Building Services Engineering Research and Technology*, 35: 69–82.

Rizwan AM, Dennis LYC, Liu C (2008). A review on the generation, determination and mitigation of Urban Heat Island. *Journal of Environmental Sciences*, 20: 120–128.

Salamanca F, Krpo A, Martilli A, Clappier A (2010). A new building energy model coupled with an urban canopy parameterization for urban climate simulations—part I. formulation, verification, and sensitivity analysis of the model. *Theoretical and Applied Climatology*, 99: 331–344.

Sharma A, Fernando HJS, Hellmann J, Chen F (2014). Sensitivity of WRF model to urban parameterizations, with applications to chicago metropolitan urban heat island. In: Proceedings of the 4th Joint US-European Fluids Engineering Summer Meeting, FEDSM2014, Chicago, USA.

Skamarock WC, Klemp JB, Dudhia J, Gill DO, Barker DM, Duda MG, Huang XY, Wang W, Powers JG (2008). A description of the advanced research WRF version 3. NCAR tech notes-475+ STR.

Spera DA, Richards TR (1979). Modified power law equations for vertical wind profiles. DOE/NASA/1 059-79/4, NASA TM-79275.

Stewart ID, Oke TR (2012). Local climate zones for urban temperature studies. *Bulletin of the American Meteorological Society*, 93: 1879–1900.

Vuckovic M, Kiesel K, Mahdavi A (2017). The extent and implications of the microclimatic conditions in the urban environment: A Vienna case study. *Sustainability*, 9(2): 177.

Vuckovic M, Maleki A, Mahdavi A (2018). Strategies for development and improvement of the urban fabric: A Vienna case study. *Climate*, 6: 7.

Wilby RL, Wigley TML (1997). Downscaling general circulation model output: A review of methods and limitations. *Progress in Physical Geography: Earth and Environment*, 21: 530–548.

WMO (2018). Guide to Meteorological Instruments and Methods of Observation, WMO-No. 8, 7th edn. World Meteorological Organization.

WRF (2018). Available at http://www.wrf-model.org. Accessed 07 Feb2018.

ZAMG (2018). Available at http://www.zamg.ac.at. Accessed 07 Feb2018.